

Robust atomic force microscopy using multiple sensors

Mayank Baranwal, Ram S. Gorugant, and Srinivasa M. Salapaka

Citation: *Review of Scientific Instruments* **87**, 083704 (2016); doi: 10.1063/1.4960714

View online: <http://dx.doi.org/10.1063/1.4960714>

View Table of Contents: <http://scitation.aip.org/content/aip/journal/rsi/87/8?ver=pdfcov>

Published by the AIP Publishing

Articles you may be interested in

[Automated force controller for amplitude modulation atomic force microscopy](#)

Rev. Sci. Instrum. **87**, 053705 (2016); 10.1063/1.4950777

[High-speed tapping-mode atomic force microscopy using a Q-controlled regular cantilever acting as the actuator: Proof-of-principle experiments](#)

Rev. Sci. Instrum. **85**, 123705 (2014); 10.1063/1.4903469

[Microcantilevers with embedded accelerometers for dynamic atomic force microscopy](#)

Appl. Phys. Lett. **104**, 083109 (2014); 10.1063/1.4866664

[Loss tangent imaging: Theory and simulations of repulsive-mode tapping atomic force microscopy](#)

Appl. Phys. Lett. **100**, 073106 (2012); 10.1063/1.3675836

[Fast imaging with alternative signal for dynamic atomic force microscopy](#)

Appl. Phys. Lett. **97**, 133101 (2010); 10.1063/1.3495987



SHIMADZU Excellence in Science **Powerful, Multi-functional UV-Vis-NIR and FTIR Spectrophotometers**

Providing the utmost in sensitivity, accuracy and resolution for applications in materials characterization and science

- Photovoltaics
- Ceramics
- DNA film structures
- Polymers
- Thin films
- Packaging materials
- Coatings
- Inks
- Nanotechnology
- Paints

[Click here for accurate, cost-effective laboratory solutions](#)



Robust atomic force microscopy using multiple sensors

Mayank Baranwal,^{a)} Ram S. Goruganti,^{b)} and Srinivasa M. Salapaka^{c)}

Department of Mechanical Science and Engineering, University of Illinois at Urbana-Champaign, Urbana, Illinois 61801, USA

(Received 23 January 2016; accepted 29 July 2016; published online 15 August 2016)

Atomic force microscopy typically relies on high-resolution high-bandwidth cantilever deflection measurements based control for imaging and estimating sample topography and properties. More precisely, in amplitude-modulation atomic force microscopy (AM-AFM), the control effort that regulates deflection amplitude is used as an estimate of sample topography; similarly, contact-mode AFM uses regulation of deflection signal to generate sample topography. In this article, a control design scheme based on an additional feedback mechanism that uses vertical z -piezo motion sensor, which augments the deflection based control scheme, is proposed and evaluated. The proposed scheme exploits the fact that the piezo motion sensor, though inferior to the cantilever deflection signal in terms of resolution and bandwidth, provides information on piezo actuator dynamics that is not easily retrievable from the deflection signal. The augmented design results in significant improvements in imaging bandwidth and robustness, especially in AM-AFM, where the complicated underlying nonlinear dynamics inhibits estimating piezo motions from deflection signals. In AM-AFM experiments, the two-sensor based design demonstrates a substantial improvement in robustness to modeling uncertainties by practically eliminating the peak in the sensitivity plot without affecting the closed-loop bandwidth when compared to a design that does not use the piezo-position sensor based feedback. The contact-mode imaging results, which use proportional-integral controllers for cantilever-deflection regulation, demonstrate improvements in bandwidth and robustness to modeling uncertainties, respectively, by over 30% and 20%. The piezo-sensor based feedback is developed using \mathcal{H}_∞ control framework. Published by AIP Publishing. [<http://dx.doi.org/10.1063/1.4960714>]

I. INTRODUCTION

The atomic force microscope (AFM) is a powerful microcantilever based device that achieves high resolution, nano-scale images of samples and is able to manipulate sample properties at atomic scale^{6,10,16,21,24,35,42} (see Fig. 1 for the general operation principle). Since its invention in 1986 by Binnig *et al.*,¹⁰ significant amount of research has aimed in increasing the imaging speed of the AFM. A significant aspect of this effort has relied on redesigning the components of AFM, such as smaller cantilevers with higher resonant frequencies, improved designs for lateral and vertical positioning stages for better positioning bandwidth, and faster electronics for high-bandwidth control implementation.^{22,34,47,50–52} Another significant area of effort has stressed on redesigning control strategies to improve the resolution, bandwidth, and reliability of AFMs. This research has spanned designing control laws for lateral positioning systems,^{11,14,25,37,40,43,44} vertical imaging components,^{15,19,36,45} new imaging techniques,^{27,29} and multi-cantilever devices.^{32,41,48} These efforts are having significant impact; for instance, recently a very interesting work by Kodera *et al.*²³ demonstrated video-rate imaging of a walking myosin V by using high-speed AFM. This is achieved by innovations on both the hardware (such as the cantilevers and the electronics) and sensing and control architecture.

However, there are still many challenges that need to be overcome to realize the full potential of AFM. One of the main challenges arises from the uncertain and nonlinear dynamics that describes the tip-sample interaction. More specifically, the current amplitude modulation-AFM (AM-AFM) has inherent nonlinear dynamics, which make it difficult to design high-bandwidth controllers; this problem is made worse by the associated nonlinearities and high-frequency dynamics of a vertical positioner.

In this paper, we provide an approach based on control redesign that aims at better reliability (robustness) of the piezo actuator, which translates into better bandwidth and robustness to uncertainties of the entire device. The central idea is to implement a cascaded control structure, where the inner control-loop exploits the linear dynamical behavior of the vertical piezoactuator and thus makes it possible for the outer-control loop to achieve higher bandwidth and robustness despite the uncertain and nonlinear cantilever dynamics. In this approach, the inner-loop control is facilitated by the vertical piezo-displacement (z -motion) sensor (also referred to as z -sensor in this manuscript); this low-bandwidth (relative to deflection sensor) sensor is not used in typical existing designs. The linear dynamics of the inner plant allows for using advanced linear control approaches (such as \mathcal{H}_∞ framework) for rejecting nonlinear and high-frequency dynamics by treating them as disturbances. An interesting aspect of this design is that even though the z -sensor is a relatively low-resolution, low-bandwidth sensor (as opposed to a superior photo sensitive device (PSD) based cantilever deflection sensor), the appropriate placement of this additional sensor in

^{a)}baranwa2@illinois.edu. URL: <http://web.engr.illinois.edu/~baranwa2>.

^{b)}gorugan2@illinois.edu

^{c)}Author to whom correspondence should be addressed. Electronic mail: salapaka@illinois.edu

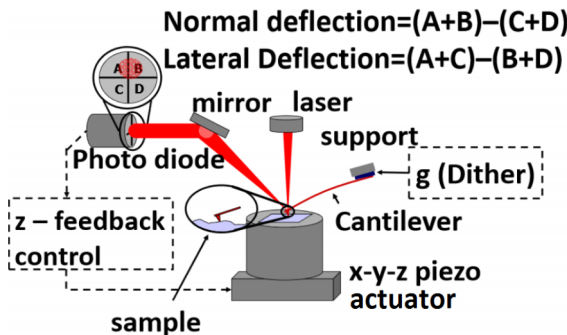


FIG. 1. In a typical AFM, the cantilever is the primary probing device. The deflection of the cantilever is measured by a photodiode sensor. There are two common modes of imaging in an AFM—(a) *Contact mode*—in contact mode of operation, it is required to maintain a constant force between the cantilever tip and the sample by maintaining a constant cantilever deflection. During constant force scans, a feedback controller acts on the photo sensitive device (PSD) voltage and actuates the vertical z -piezo-actuator to regulate the voltage to a constant set point. This kind of regulation ensures constant cantilever deflection. The control input to the piezoactuator provides a measure of the sample topography. (b) *Amplitude modulated-AFM (AM-AFM)*—in AM-AFM imaging, the cantilever is sinusoidally actuated by the dither input at a frequency ω close to its natural frequency and the change in amplitude of cantilever due to sample interaction is exploited. The deflection signal of the cantilever is passed through a lock-in-amplifier to obtain the *amplitude* and *phase* of its oscillation. The controller then regulates the amplitude signal to a constant set-point value by moving the z -piezo actuator and this control signal serves as a measure of the sample topography.

the overall control-scheme results in improved performance and robustness. This design is more effective in AM-AFM, where severe challenges are imposed by the nonlinear relationship between the input to the piezoactuator and the amplitude of the cantilever oscillations.

Another interesting aspect of this work is the use of relatively new technology known as the field programmable analog arrays (FPAs)⁷ for implementing high-bandwidth controllers. FPAs have emerged as interesting alternatives to their digital counterparts for most signal processing based applications. In FPAs, a fully differential switched capacitor architecture³ allows integration of a larger number of elements per chip and provides high precision and high efficiency when compared to digital signal processors (DSPs). It is relatively simple to implement transfer function (which is the ratio of the output of a system to the input of a system in the frequency domain) using FPAs with reconfigurable networks of op-amps based circuits; moreover, FPA technology is relatively very inexpensive. In our work in Refs. 8 and 9, FPA based controller implementation results show 200% improvement in tracking bandwidth over a conventional high-performance DSP based implementation, wherein we show the efficacy of FPAs for implementing high-order, high-bandwidth controllers.

The rest of the paper is organized as follows. Section II puts forth the objectives of the proposed work and describes the key challenges associated with high-speed, model-based control designs. We then discuss the control of inner- z loop, followed by a section on theoretical and experimental results for AFM imaging using the proposed inner-outer framework. The discussion is finally concluded with a summary of the key results.

II. PROBLEM FORMULATION AND SOLUTION

In this paper, we present our analysis and design in terms of transfer function block diagrams as shown in Fig. 2. In this figure, G_z is the transfer function of the z -positioner comprising the actuator, flexure stage, and sensor. It represents a dynamical relationship between its output, the flexure stage displacement z , and its input, the voltage u given to the actuator (see Fig. 2(b)). Similarly, G_c represents the transfer function of the cantilever assembly comprising the tip-holder, dither actuator, and the PSD sensor. The signals d , n , and y represent disturbance due to sample-profile, the sensor noise, and the cantilever-tip deflection (in PSD voltage), respectively. The signals r and y_m represent the reference and the measured output, respectively (deflection for contact-mode, amplitude for AM-AFM). Ψ is a functional block, which acts as identity for contact-mode operation and as amplitude-detector for AM-AFM operation. K is the transfer function of the controller.

The objectives of this work are two-fold. First, we aim to improve the performance and robustness of the vertical z -piezo actuator by designing a closed-loop feedback controller using the available z -sensor (see Fig. 2(b)). Second, we investigate the advantages of incorporating thus modified z -piezo actuator in the conventional control scheme for reliable AFM imaging, i.e., we investigate the significance of adding the inferior z -sensor for contact and AM-AFM imaging. In the proposed

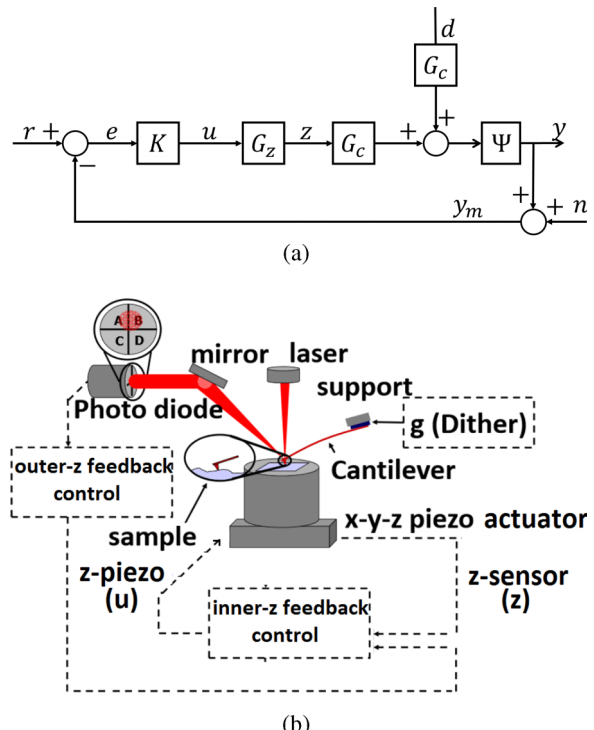


FIG. 2. (a) Block diagram schematic for AFM imaging system with no z -sensor feedback. Here Ψ represents a functional block which is identity for contact-mode imaging and a non-linear amplitude-detection block for AM-AFM imaging. The reference signal, r is a deflection set-point for contact-mode imaging and amplitude set-point for AM-AFM imaging. Similarly, the measured output, y_m represents deflection of the cantilever tip for contact-mode imaging and amplitude of oscillation of the cantilever tip for AM-AFM operation. (b) Proposed control scheme with inner-outer control architecture. Notice that this scheme uses the z -sensor for inner-loop control contrary to conventional AFM control as shown in Fig. 1.

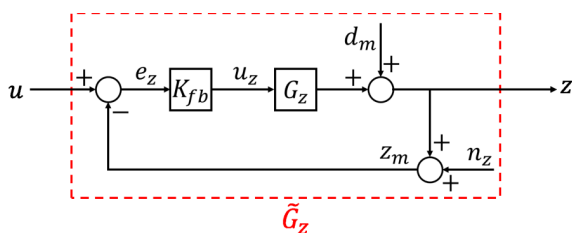


FIG. 3. Block diagram schematic for the modified inner- z piezo actuator. Note that the proposed cascaded control scheme *replaces* the actual z -piezo actuator G_z (shown in Fig. 2(a)) with a suitably modified plant \tilde{G}_z that aims to mitigate the effects of uncertainties in piezo actuator motion. K_{fb} represents the transfer function for the inner-controller. Here, the signals u and z carry the same meanings as in Fig. 2(a). e_z is the error in tracking the commanded input u , while d_m represents the mechanical noise such as drift, creep, and hysteresis. n_z is the sensor-noise in the z -displacement measurement.

approach, the inner- z controller is designed to attenuate the effects of high-frequency dynamics of the z -piezo actuator (particularly in AM-AFM), while the outer-controller is designed to achieve the overall reference tracking. This approach is motivated by *inner-current outer-voltage* control for voltage inverters, where the inner controller is designed to achieve fast rejection to disturbance in current arising due to variations in the output load, while the primary outer controller regulates the output power/voltage by generating the required set-point for the inner loop.³⁸

We aim to design a feedback controller K_{fb} for the z -piezo actuator G_z that makes the tracking error small, attenuates effects of sensor noise, and is robust to modeling uncertainties (shown in Fig. 3). In Ref. 26, it is demonstrated in Fig. 10(a) that the frequency responses of a piezo actuator vary at different operating points. The variation in the responses is indicative of the modeling errors (uncertainties) in the identified plant. In addition, it is also observed that the frequency response at the same operating point varies when obtained at different times. In view of these uncertainties, robustness of the closed-loop z -piezo actuator is a critical requirement of control design. We denote the closed-loop z -piezo actuator plant by \tilde{G}_z . The closed-loop plant \tilde{G}_z is shown in Fig. 3. Note that the deflection y_m has information on the piezo actuator motion z through the *nonlinear* tip-sample interaction Ψ and sample profile d . Therefore, it is difficult for any control action that depends only on y_m to attenuate the effects of uncertainties in piezo actuator. The piezo sensor motion z_m based control on the other hand (shown in Fig. 3) is much better suited to address these effects.

From this figure, we have

$$\begin{aligned} \text{Tracking error, } e_z &= S(u - n_z), \\ \text{Output displacement, } z &= G_z K_{fb} e_z = T(u - n_z), \\ \text{Control input, } u_z &= K_{fb} e_z = K_{fb} S(u - n_z), \quad (1) \\ S &= (1 + G_z K_{fb})^{-1}, \\ \text{and } T &= G_z K_{fb} (1 + G_z K_{fb})^{-1}, \end{aligned}$$

where the sensitivity transfer function S is the closed-loop transfer function from reference u to tracking error e_z and measures the robustness of the closed-loop system to modeling and parametric plant uncertainties, and the complementary sensitivity transfer function T is the closed-loop transfer func-

tion from reference u to the displacement z (and from noise n_z to displacement z).

There are fundamental limitations on the achievable specifications, which regardless of the control design, cannot be overcome.^{26,46} For instance, due to the algebraic constraint, $S + T = 1$, increasing the bandwidth of S would mean that T would still be large for relatively higher frequencies. This in turn would result in significant amplification of high-frequency noise, thereby resulting in poor positioning resolution. The closed-loop transfer function $K_{fb}S$, which represents the dynamical relationship between e_z and the controller output u_z , needs to be bounded (since the maximum absolute drive voltage to piezoactuators in an AFM is bounded) in order to avoid effects such as saturation and equipment damage. In the context of piezoactuated stages, these conflicting objectives are addressed in optimal, model-based configuration using modern \mathcal{H}_{∞} -control framework.^{26,30,31}

Having now discussed the various fundamental constraints with the inner-loop control design, it still remains unclear whether the improved inner-loop enhances the performance of the outer-loop. This becomes even more relevant in the case of AFMs, where the additional z -sensor is relatively inferior to the cantilever-tip displacement sensor in terms of resolution (~0.5 nm average deviation for z -sensor compared to <0.02 nm for photodiode sensor) and bandwidth (~10 kHz for z -sensor compared to 2 MHz for photodiode sensor). Fig. 4 shows the frequency response of the vertical z -piezo actuator in an MFP-3D AFM. The identification is performed using NI LabVIEW²⁰ and an NI PCIe-6361 DAQ card.² From the figure, one can observe sharp peaks at ~1 kHz and ~2 kHz. This in turn implies that the output response of the z -piezo actuator gets amplified at these frequencies. Hence, if the z -piezo actuator is left uncontrolled, the effect of this high-frequency behavior gets propagated to other parts of the plant, thereby resulting in spurious and unreliable imaging. In conventional AFM imaging, this problem is partially alleviated by designing low-bandwidth PI controllers with very small gains at high-frequencies, thus restricting the bandwidth of the closed-loop system. The nonlinear dynamics of the plant, particularly in AM-AFM, which use only deflection measurements, make it difficult to design controllers for disturbance rejection at these frequencies. While the approach proposed in this work employs inner- z control to mitigate the effects of the high-frequency dynamics, *high-bandwidth* PI controllers are designed to control the outer-loop, thus allowing faster scan rates.

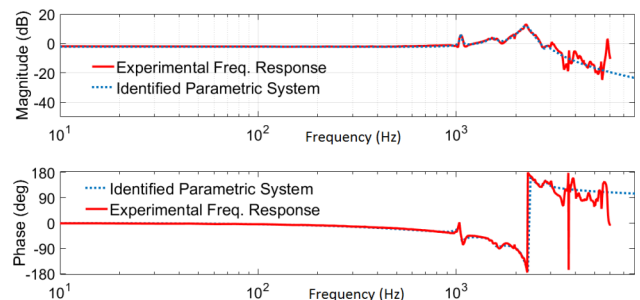


FIG. 4. Experimental frequency response of the vertical z -piezo actuator in MFP-3D AFM and linear parametric fit to the experimental data in the operating frequency range.

III. CONTROL DESIGN

The design of control laws for achieving *simultaneously* the above objectives renders tuning based control designs (PI/PII) impractical and ineffective. Therefore, we employ tools from the modern robust control-theoretic framework, where an optimal controller K over a set \mathcal{K} of proper, stabilizing controllers is sought by posing a feasible optimization problem for a given set of design specifications. The main advantage of this approach is that the performance objectives can be directly incorporated into the cost function. These optimization problems are of the form,

$$\min_{K \in \mathcal{K}} \|\Phi(K)\|_\infty, \quad (2)$$

where Φ is a matrix transfer function, whose elements are in terms of the closed-loop transfer functions (such as in Eq. (1)). For example, Φ represents a matrix transfer function from *external* variables, such as reference command and sensor noise, to *regulated* outputs, such as tracking error and control signal. In this case, minimizing $\|\Phi\|_\infty$ is equivalent to making the ratio of the magnitudes of regulated variables to external variables small, regardless of the external signals (i.e., the optimization problem seeks to minimize the worst case gain from disturbance inputs to system outputs). These optimization problems have been studied extensively in Refs. 46 and 12 and can be solved efficiently using standard MATLAB¹⁸ routines. In this section, we present \mathcal{H}_∞ -control designs for the above goals using the *Glover-McFarlane robust loop-shaping approach*.^{17,30}

Even though some piezoactuated positioning stages with pre-defined feedback controllers exhibit satisfactory resolution and tracking bandwidth at designed operating conditions, a slight deviation from these operating conditions may result in rapid degradation in tracking performance sometimes resulting in system instability. This is indeed true with many flexure-based mechanisms which are very lowly damped and are close to being marginally stable. The Glover-McFarlane framework allows us to first design controllers for high closed-loop bandwidth and later incorporate the robustness by characterizing the specific form of uncertainty. In Ref. 44, authors used Glover-McFarlane method^{17,30} to design control laws, which wrapped around pre-existing controllers that resulted in significant improvements in robustness.

Fig. 5 shows the block-diagram for a robust loop-shaping Glover-McFarlane control design. In this framework, the given plant G_z is first pre-compensated using W_1 , so that the gain of the *shaped-plant*, $G_S = G_z W_1$ is sufficiently high at frequencies where good disturbance attenuation is required and is

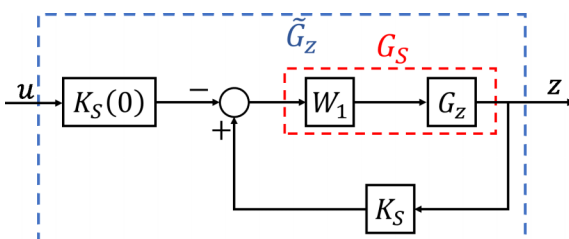


FIG. 5. A Glover-McFarlane robust loop-shaping control framework with pre-compensator W_1 .

sufficiently low at frequencies where good robust stability is required. The robustness condition is imposed by requiring the controller to guarantee stability for a set of transfer function models that are “close” to the nominal model G_S . The resulting optimal controller guarantees the stability of the closed-loop positioning system, where the shaped-plant is represented by any transfer function G_p in the set,

$$\{G_p = (M - \Delta_M)^{-1}(N + \Delta_N), \|[\Delta_M \quad \Delta_N]\|_\infty \leq \gamma^{-1}\}, \quad (3)$$

where $G_S = M^{-1}N$ is a coprime factorization,⁴⁹ $[\Delta_M \quad \Delta_N]$ represents the uncertain dynamics, and γ specifies a bound on this uncertainty. While the nominal shaped plant $G_S = M^{-1}N$ is deemed stable, the uncertainty set in Eq. (3) may still include plants that are marginally stable to even unstable. This characterization of uncertainty is particularly relevant to nanopositioning systems, which typically have very low damping; uncertainties in plant parameters for such systems are well addressed by the uncertainty set in Eq. (3). Moreover, for a shaping controller K_S , the minimum possible γ can be calculated *a priori*.

IV. INNER-LOOP CONTROL USING GLOVER-MCFARLANE ROBUST LOOP-SHAPING

The frequency response of the vertical z -piezo actuator in our MFP-3D AFM is obtained using standard system identification methods, such as the blackbox identification method.²⁸ A sine sweep signal, over a desired frequency range, is provided to the system and the z -sensor output is measured. A transfer function model is then fit to this experimental input-output data using MATLAB *invfreqs* command. Weighted iterative least square fitting was performed over 0–2 kHz, and the reduction through balanced realization¹³ resulted in the following 9th-order parametric model (see Fig. 4):

$$G_z = \frac{-2683.3(s + 1.779 \times 10^4)(s - 2.261 \times 10^4)}{(s + 7242)(s^2 + 136.7s + 4.4 \times 10^7)} \times \frac{(s^2 + 337.4s + 4.394 \times 10^7)(s^2 + 1689s + 1.006 \times 10^8)}{(s^2 + 1227s + 9.563 \times 10^7)(s^2 + 1729s + 1.999 \times 10^8)} \times \frac{(s^2 + 578.2s + 3.083 \times 10^8)}{(s^2 + 748.9s + 3.119 \times 10^8)}. \quad (4)$$

In conventional AFM imaging, in order to maintain a constant set-point (deflection/amplitude), typically an integral action is provided at the input of the z -piezo. In our approach for inner-loop control, the z -piezo actuator is first filtered through a modified PI precompensator W_1 . The precompensator W_1 is chosen, so that the shaped-plant $G_S = G_z W_1$ has the desired integral action (high-gain at low-frequencies) and a small-gain near resonant frequency (but, not small enough to lower the bandwidth of the shaped-plant). The shaped-plant is then subjected to a closed-loop control using the Glover-McFarlane robust loop-shaping method.^{17,30} A remarkable feature of this design is that it achieves *robustness* with marginal reduction in performance. In fact, it is able to quantify the reduction by determining explicit bounds on how much it changes the loop gains at low and high frequencies. The precompensator W_1 was chosen to be $5000/(s + 10)$. The Glover-McFarlane design results in the following 9th-order controller. The resulting

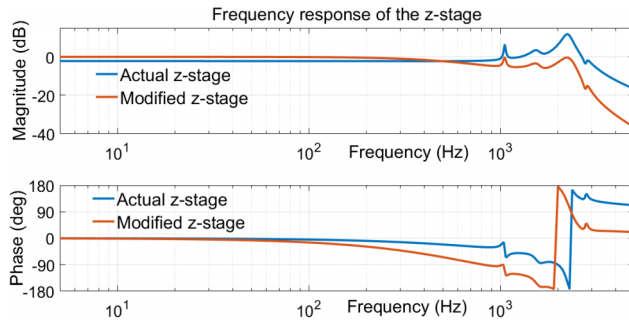


FIG. 6. Bode-plots of the open-loop and the closed-loop plants. The closed-loop system has small gain at the resonant frequency. Moreover, the closed-loop transfer function rolls-off faster at high-frequencies.

system ensures robustness with *gain-margin* of 9.92 dB and *phase-margin* of 80.3°,

$$K_S = \frac{-1.5299(s + 7397)(s^2 + 68.32s + 4.349 \times 10^7)}{(s + 1.116 \times 10^4)(s^2 + 314.3s + 4.374 \times 10^7)} \\ \times \frac{(s^2 + 1114s + 9.417 \times 10^7)(s^2 + 320.3s + 1.967 \times 10^8)}{(s^2 + 1664s + 9.896 \times 10^7)(s^2 + 8209s + 2.928 \times 10^8)} \\ \times \frac{(s^2 + 752.8s + 3.12 \times 10^8)}{(s^2 + 749.5s + 3.095 \times 10^8)}. \quad (5)$$

Fig. 6 shows the frequency response of the open-loop plant G_z and the closed-loop plant \tilde{G}_z . The closed-loop plant has a suppressed peak at the resonant frequency of the z -piezo actuator. Moreover, the closed-loop transfer function rolls-off faster without noticeable reduction in performance or bandwidth. A constant gain block is added during implementation to ensure 0 dB steady-state gain. The controller is implemented using field programmable analog arrays (FPAs),⁴ which have a direct bandwidth advantage over a very high-performance DSP.³³

Fig. 7 shows the experimental tracking response of the closed-loop system for a small-amplitude noisy 20 Hz sinusoidal reference and a 500 Hz (band-unlimited) triangular reference signals, respectively. While in Fig. 7(a), the closed-loop response is shown to be practically insensitive to signal noise, and Fig. 7(b) demonstrates the efficacy of the control design in practical elimination of high-frequency component (~1.5 kHz) observed in the open-loop case. This is due to the flatter response of the closed-loop system when compared to the open-loop system as seen in Fig. 6.

Note: Fig. 8 shows the experimental noise spectrum of the z -sensor and follows the typical $1/f$ -noise (also known as Johnson noise). It is often believed that incorporating an additional noisy sensor necessarily degrades the performance of the overall system. While this may be true for certain systems whose exact parametric models are available, this is certainly not the case with most piezo-based systems. Let us denote the effects of uncertainties in dynamics of the z -piezo actuator as *mechanical noise*. The proposed feedback-based approach allows a trade-off between mechanical and sensor noise. Moreover, large separation between the resonant frequencies of the cantilever (ω_c) and the z -piezo (ω_z) ensures that the effect of z -sensor noise on the cantilever deflection is practically negligible. This can be understood as follows. For “acceptable” topography measurement, it is

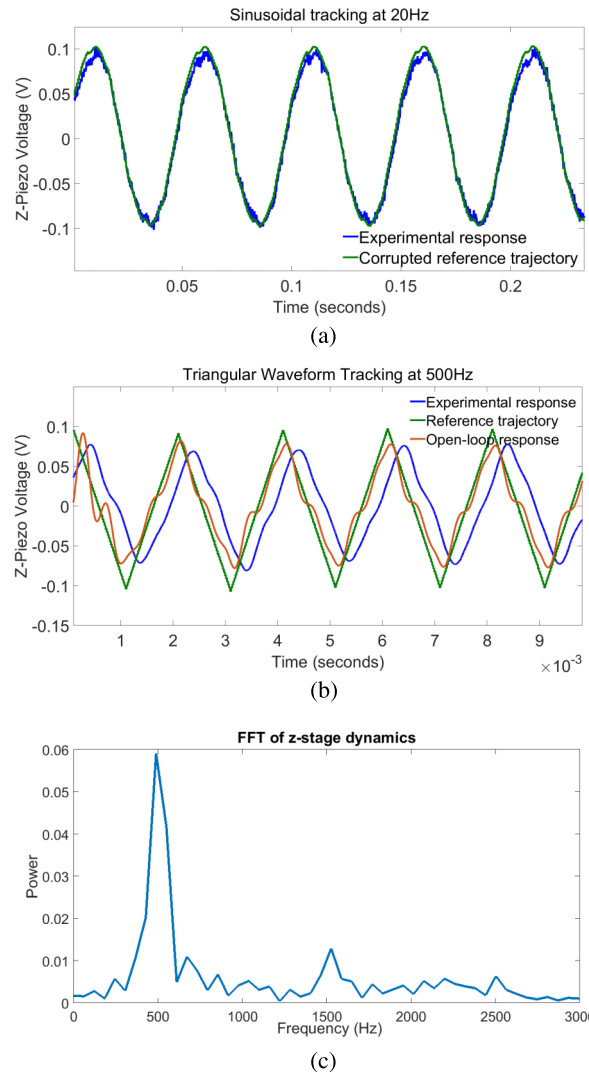


FIG. 7. Experimental tracking response of the FPA based implementation of Glover-McFarlane robust loop-shaping control design for the vertical z -piezo actuator. (a) Tracking response to noisy 20 Hz sinusoidal signal. The tracking response is practically insensitive to signal noise, i.e., the effect of z -sensor noise is imperceptible (compared to the original signal). (b) Open-loop and closed-loop response to 500 Hz triangular signal. It can be seen that there is a high-frequency (1.5 kHz) signal riding on the 500 Hz component for the open-loop response, which in turn shows the effect of the high-frequency dynamics. Since, the z -sensor output is used as a measurement signal for topography estimation in AFM imaging, the high-frequency behavior results in spurious image construction. (c) FFT of the output response of open-loop plant.

required that the lateral bandwidth ω_l (proportional to number of sample features per unit time) is smaller than the vertical (z) positioning bandwidth ω_z . Without loss of generality, let us assume that the amplitude of the deflection signal at time t due to variation in sample profile is given by $A(t) = \cos(\omega_l t)$, while the cantilever oscillates at its resonant frequency ω_c . Thus, the cantilever deflection is approximately (disregarding minor variations in resonant frequency due to tip-sample interaction) given by $y(t) = \cos(\omega_l t) \cos(\omega_c t + \phi) = \cos((\omega_c + \omega_l)t + \phi) + \cos((\omega_c - \omega_l)t + \phi)$, where ϕ is the steady-state phase difference due to tip-sample interaction. Since $\omega_c \gg \omega_l$ and the sensor noise is inversely proportional to the frequency, the effect of noise at frequencies ($\omega_c + \omega_l$)

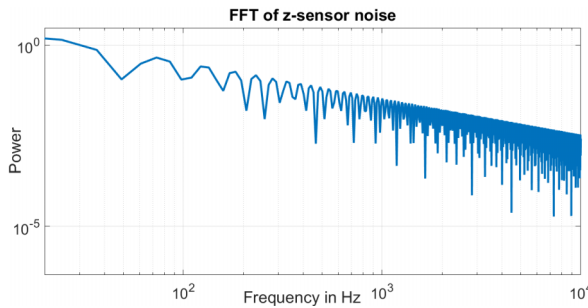


FIG. 8. Power spectrum of z -sensor noise. As expected, the sensor noise follows the well-known Johnson noise ($1/f$ noise).

and $(\omega_c - \omega_l)$ is practically negligible. This is corroborated by our experiments too, as we did not observe any visual change in the deflection sensor noise with and without the inner-loop control.

V. OUTER-LOOP CONTROL FOR AMPLITUDE REGULATION IN AM-AFM IMAGING

In AM-AFM imaging, an outer-loop controller maintains a constant amplitude set-point by regulating the displacement of the z -piezo actuator (without any inner control). The choice of outer-loop control is limited to PI (or its variant), primarily due to the complex and uncertain cantilever amplitude dynamic models. However, from Fig. 6, it is evident that in the absence of inner- z control, one has to contend with low-bandwidth imaging (closed-loop control) in order to avoid the effects of the high-frequency dynamics of the z -piezo actuator. The effect can be observed in the open-loop response of the z -piezo actuator for a 500 Hz triangular input signal (see Fig. 7(b)), where a high-frequency behavior sits atop the 500 Hz component. The associated nonlinearities with amplitude dynamics make it difficult to estimate the effects of the high-frequency dynamics, and thus, these effects cannot be separated from the true topography measurements. Hence, a high-bandwidth outer-loop control with no inner-control leads to spurious imaging results, due to the unsuppressed high-frequency z dynamics.

Fig. 9 shows the block diagram for the proposed *inner-outer* control framework for AM-AFM imaging. The inner-controlled loop is denoted by \tilde{G}_z . For outer-control design, we treat G_{zA} , the transfer function from output u of the controller to amplitude y , as a plant and design controller K so that the amplitude y is regulated at a constant r . Note that the plant

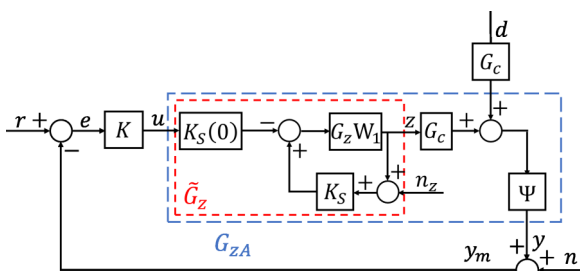
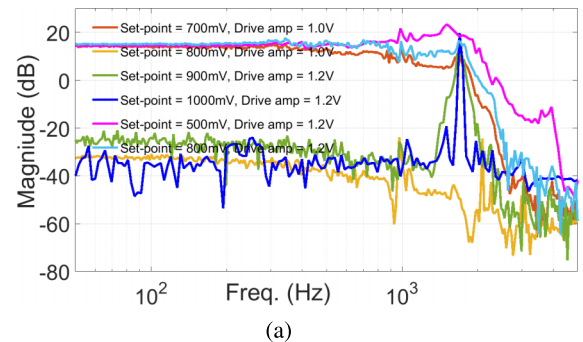
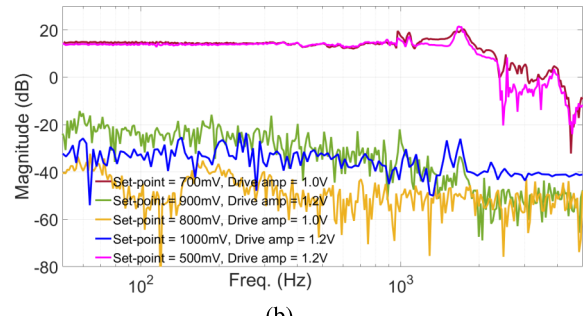


FIG. 9. Block diagram representation of control scheme for AM-AFM imaging.



(a)



(b)

FIG. 10. Experimental frequency response for the plant G_{zA} with (a) no inner-loop control - effect of high-frequency dynamics is both noticeable and unpredictable, (b) Glover-McFarlane controller for the inner-loop - effect of high-frequency dynamics is virtually non-existent. The frequency response plot with large magnitude values suggest *hard* engagement between the tip and the sample, whereas the low magnitude values are the results of *soft* engagement.

G_{zA} described in this context is nonlinear and exhibits different dynamical behavior at different operating points. Fig. 10 shows the experimental frequency response of the plant G_{zA} for the two cases—(a) no inner-loop control: as evident from Fig. 10(a), there is an abrupt change in the system gain at frequencies (~ 1 kHz) and (~ 2 kHz); moreover, the effect of the high-frequency behavior is unpredictable for different amplitude set-points and in-air drive amplitudes, (b) with inner-loop control: with the proposed Glover-McFarlane controller with the appropriately chosen precompensator, the effect of high-frequency dynamics becomes virtually non-existent. For this experiment, we used AC240TS cantilever probe⁵ with a nominal resonant frequency of 76 kHz and nominal spring constant 2 N/m.

We now investigate the effect of inner- z control for designing outer-loop controller. In AM-AFM imaging, nonlinear amplitude dynamics prevent the use of linear model-based controllers for the outer-loop. We therefore restrict ourselves to designing integral controllers for the outer-loop. Moreover, the plant dynamics changes with variations in amplitude set-points and cantilever drive amplitudes (due to associated nonlinearities in tip-sample interactions). Hence for both the cases (i.e., with or without inner-loop control), we first design outer controllers for the plants that depict *hard* engagement between the cantilever-tip and the sample represented by the set-point (s.p.) = 500 mV and drive-amplitude (d.a.) = 1.2 V and employ the same control laws to study the cases where the cantilever is softly engaged to the sample represented by the set-point (s.p.) = 900 mV and drive-amplitude (d.a.) = 1.2 V.

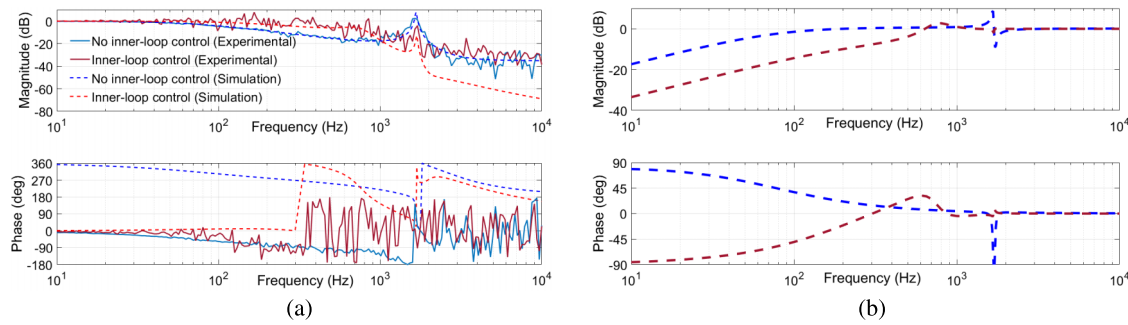


FIG. 11. Closed-loop frequency responses for the case of hard-engagement. (a) Experimental and simulated complementary sensitivity transfer functions—in the conventional AM-AFM imaging with no inner-loop control, the overall set-point to amplitude dynamics is adversely affected at the resonant frequency of the z -piezo actuator. (b) Simulated sensitivity transfer functions—the sensitivity peak is practically eliminated for the proposed design.

For the sake of fair comparisons in robustness, exhaustively tuned integral outer-controllers are tested to achieve similar bandwidths (~ 200 Hz) for the scenario of hard-engagement and for the two cases—(1) *no control on z-piezo actuator*—the optimal integral controller is obtained as $K_1 = \frac{500}{s}$, (2) *Glover-McFarlane control on z-piezo actuator*—the resulting integral controller is obtained as $K_2 = \frac{395}{s}$.

Fig. 11(a) shows the experimental and simulation closed-loop responses for the conventional (no inner-loop control) and the proposed (with inner-loop control) approach for the hard-engagement scenario. The experimental and simulation responses corroborate the usefulness of the proposed inner-outer control design. In the conventional AM-AFM imaging with no inner-loop control, the overall set-point to amplitude dynamics is adversely affected at the resonant frequency of the z -piezo actuator, which is seen clearly in the experimental closed-loop complementary sensitivity transfer function in Fig. 11(a). This is also observed in Fig. 11(b) for the proposed design, where the peak in the sensitivity plot is practically eliminated, thereby allowing a very high gain margin and making the design practically insensitive to modeling uncertainties. The controllers K_1 and K_2 are then tested for the scenario, where the cantilever-tip is softly engaged to the sample (see Fig. 12). Note that in this scenario, the controller results in relatively much smaller closed-loop bandwidths as the system gains are very small in the frequencies of operation. However, a small peak near the resonant frequency of the z -piezo actuator in the sensitivity plot (see Fig. 12(b)) is still observed for the plant with no inner-control, thereby indicating slightly poor robustness around those frequencies.

Remark: Note that the proposed inner-outer control scheme does not have any significant advantage over the conventional control scheme for the scenarios that capture excessively soft engagements between the cantilever-tip and the sample (shown by orange curve in Fig. 10(a)). This is primarily due to very small frequency-response gains (see Fig. 10(a)), resulting in closed-loop transfer functions that die off much below the resonant frequency of the z -piezo actuator. However, the proposed approach still outscores the conventional approach for moderately soft engagements (as shown in Fig. 12). Thus the proposed design is particularly useful for scenarios that correspond to hard to moderately soft engagement between the tip and the sample. However, it should be remarked that any practical imaging will require sufficiently hard engagement between the tip and the sample.

Application of the proposed approach for contact-mode imaging: A similar comparison exists for contact-mode AFM imaging with PI controller for the outer loop, as is the case with usual contact-mode imaging. We used contact-mode silicon probe¹ with resonant frequency ~ 13 kHz. Exhaustively tuned PI controllers are derived using MATLAB/Simulink for the two cases—(1) *no control on z-piezo actuator*—the PID tuner block resulted in the following optimal PI controller, $K = \frac{1902.27}{s}$. The resulting closed-loop bandwidth was 234 Hz, with a peak sensitivity value of 4.34 dB. (2) *Glover-McFarlane control on z-piezo actuator*—the optimal control law in this case was $K = 0.102 + \frac{2068}{s}$. The resulting closed-loop bandwidth and peak sensitivity values were 315 Hz and 3.37 dB, respectively. Thus, a 34.79% improvement in tracking bandwidth and a 22.35% decrease in peak sensitivity values (a

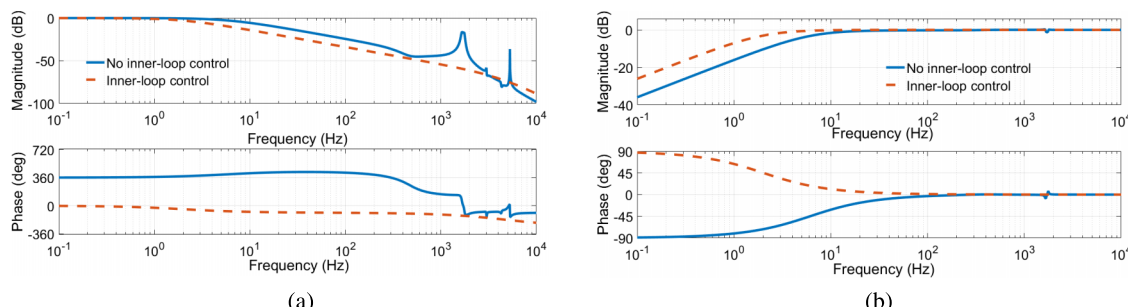


FIG. 12. Closed-loop transfer functions for the case of soft-engagement. (a) Complementary sensitivity transfer functions—the effect of the z inner-loop actuator dynamics is clearly seen in the uncontrolled z inner-loop case. (b) Sensitivity transfer functions—there is no observable sensitivity peak for the proposed approach.

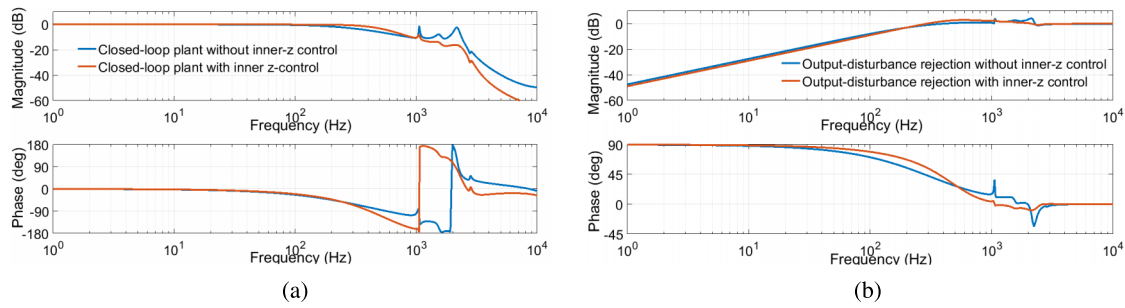


FIG. 13. Complementary sensitivity and sensitivity transfer functions for the closed-loop control of contact-mode imaging. (a) The complementary sensitivity plot for the controlled inner-loop (red) rolls-off faster at high frequencies; moreover, the achievable bandwidth is higher than in the case of uncontrolled z -piezo actuator (blue). (b) The sensitivity plot for the controlled inner-loop case (red) lies below the sensitivity plot for the uncontrolled z -piezo actuator case (blue) for frequencies below the crossover frequency. Moreover, there is a sharp peak near the resonant frequency of the z -piezo actuator in the latter case, thereby degrading robustness at those frequencies.

measure for robustness^{40,46}) were obtained with the modified z -plant. Fig. 13 shows the closed-loop sensitivity and complementary sensitivity transfer functions for the two cases.

However, we must specify that it is still possible to achieve comparable performance and robustness for contact-mode imaging without the need for additional z -control, as shown in Ref. 39. This is mainly due to the availability of linear plant models and a wide separation in the resonant frequencies of the contact-mode cantilever and the vertical z -piezo actuator. Modern \mathcal{H}_∞ based outer-controllers are designed in Ref. 39 to eliminate the effects of high-frequency dynamics of the z -piezo actuator without having to include additional z -sensor in the overall control scheme.

Tapping-mode AFM imaging using the proposed inner-outer design and comparisons with the usual tapping-mode: We now discuss the advantages of the proposed modified z -piezo actuator for AFM imaging. As discussed earlier, the proposed design renders the closed-loop imaging system *insensitive* to small variations in set-points and scanning speeds as compared to the usual tapping-mode imaging, where the z -piezo actuator is left uncontrolled. The effects of the proposed design are reflected in AFM images through *sharpness* of features and *improved* trace-retrace characteristics. A calibration grating with $5\mu\text{m} \times 5\mu\text{m}$ pitch and 25 nm feature height is considered for experimental comparison of the two

approaches. The outer controllers are tuned exhaustively for the two scenarios (with and without inner-loop control), and the scans are obtained at varying set points and scanning speeds.

Fig. 14 shows section (line) scans of the calibration grating along the x -direction at a set-point of 800 mV and scan-speed of 20 Hz. Clearly the proposed approach results in better estimates of the feature heights (25 nm), whereas the usual tapping-mode images of the *same* feature provide *inaccurate* information about the feature dimensions (~ 30 nm). Moreover, the feature reconstruction is relatively *sharper* in the case of tapping-mode imaging with inner-loop control (see Fig. 14(c)).

As stated earlier, the outer PI controllers for the two scenarios—with and without inner-loop control, are tuned for comparable performances at a nominal set-point of 600 mV and a scan-speed of 20 Hz. This is reflected in the excellent trace-retrace characteristics along the x -direction (as shown in Figs. 15(a) and 15(d)). While the feature heights and shapes, and trace-retrace plots are indistinguishable for a low-speed scan, the proposed control design with an inner-loop control on the z -piezo actuator results in improved performance for faster scan—100 Hz (see Figs. 15(b) and 15(e)) with sharper borders. The region of interest in the calibration simple has some anomalies and is also confirmed through a low-speed scan in Fig. 16. Note that such anomalies are seen as high-frequency

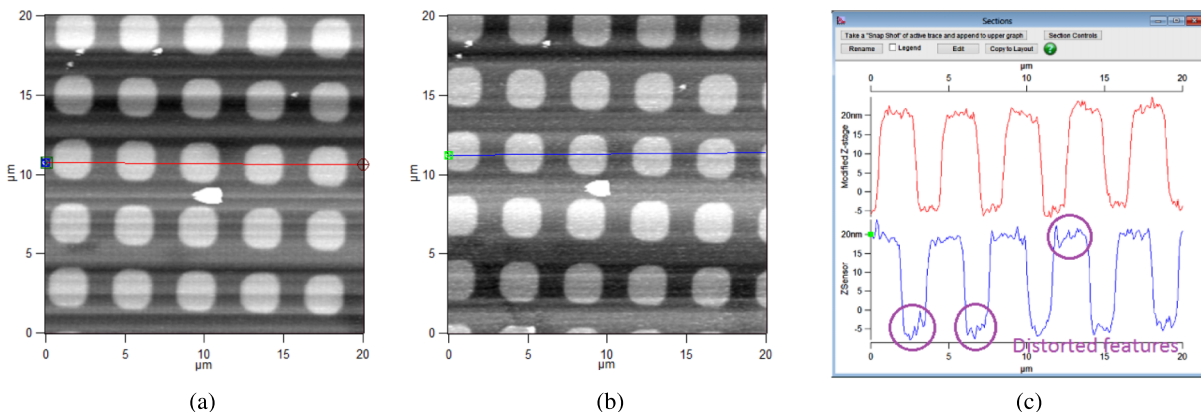


FIG. 14. Section scans of a calibration grating using (a) the proposed modified z -piezo actuator control and (b) without inner-loop control. (c) The proposed approach provides better estimates of the feature dimensions with sharper profile.

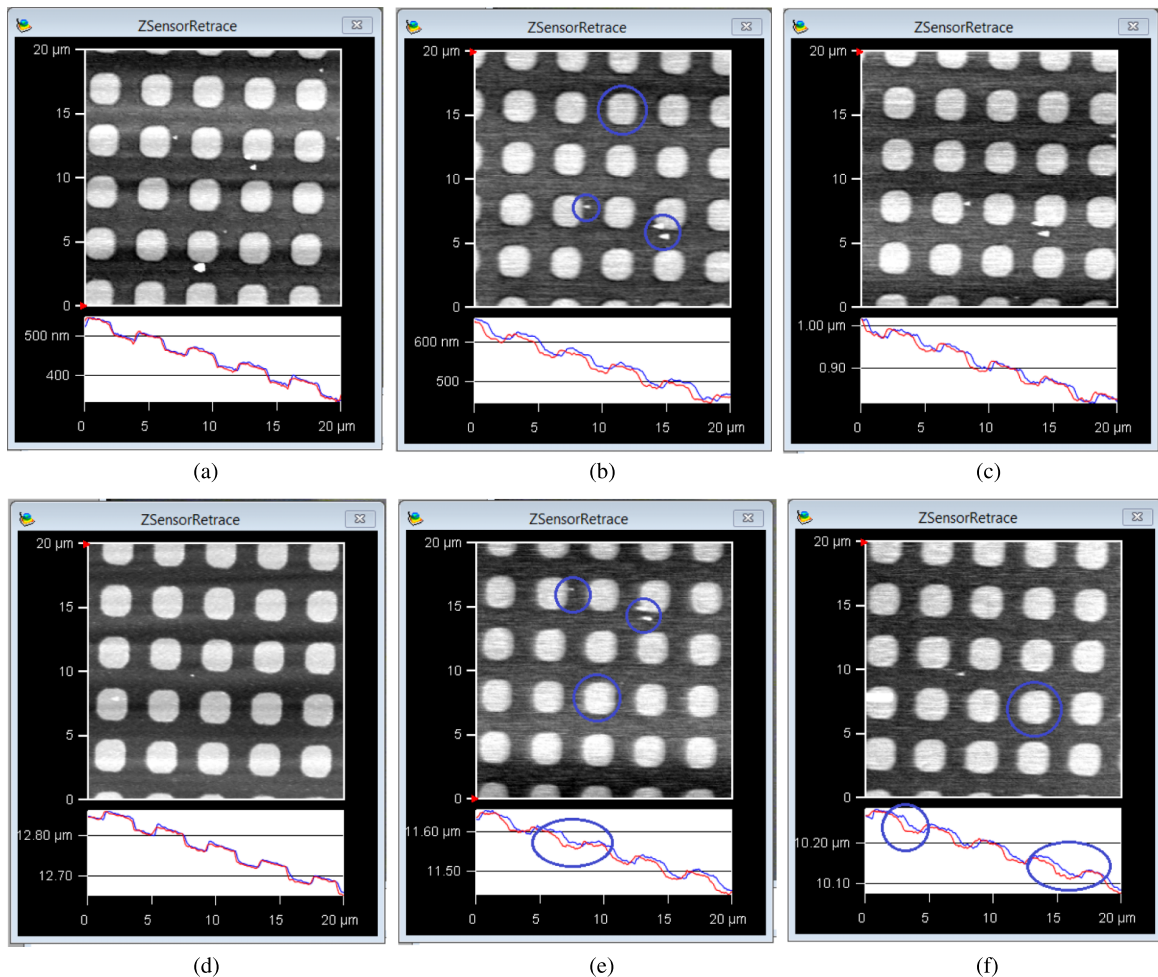


FIG. 15. Imaging results at different scan-speeds and set-points - with inner-loop control (a) set-point = 600 mV, scan-speed = 20 Hz, (b) set-point = 600 mV, scan-speed = 100 Hz, (c) set-point = 800 mV, scan-speed = 60 Hz; without inner-loop control (d) set-point = 600 mV, scan-speed = 20 Hz, (e) set-point = 600 mV, scan-speed = 100 Hz, (f) set-point = 800 mV, scan-speed = 60 Hz. While the feature heights and shapes, and trace-retrace plots are indistinguishable for a low-speed scan, the proposed control design with modified z-piezo actuator results in improved performance for faster scan and variable set-points. This is seen through the *sharper* features and *better* trace-retrace characteristics.

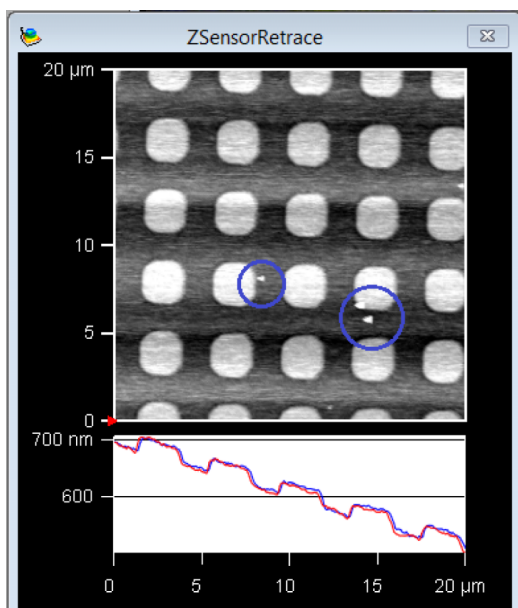


FIG. 16. Low-speed scan revealing the presence of anomalies in the calibration grating (marked by circles).

signals by the cantilever, and therefore, we expect them to be suitably revealed in the scan obtained using the proposed inner-outer approach. While these anomalies appear sharper in the scans obtained using the proposed approach (Fig. 15(b)), the usual tapping mode image (Fig. 15(e)) contains only faded appearance of them. Moreover, the trace-retrace plot shows that some of the features appear almost *flat* in the usual tapping mode scan. This is also captured by the Bode plot in Fig. 11(a), where the usual tapping-mode imaging system (with no inner-loop control) has smaller gain at 100 Hz, whereas the proposed approach with inner-loop control still has 0 dB gain at 100 Hz scanning bandwidth.

We now compare the two approaches for the scenario, where the two systems have the same 0 dB gain at low scanning frequency (60 Hz), but exhibit soft engagement between the cantilever tip and the sample (set-point 800 mV). As before, the proposed approach highlights features with clearly distinguishable (sharp) boundaries (Fig. 15(c)), while the boundaries are less sharp in the usual tapping-mode scan (Fig. 15(f)). Moreover, some of the features appear *flat* in the trace-retrace plots of the usual tapping-mode scan with large values of trace-retrace mismatch.

VI. CONCLUSION

In this work, we focus on improving the imaging bandwidth, particularly in AM-AFM, by attenuating the effects of high-frequency dynamics in the vertical z -piezo using multiple-sensors. A cascaded *inner-outer* control framework is proposed in which an inner- z controller is designed to minimize the effects of high-frequency dynamics which manifest as spurious features in images. We thus demonstrate that a relatively inferior z -sensor, when placed appropriately in the overall control scheme, results in improved imaging performance. Tools from robust control theory are employed to design optimal, model-based controller for the z -piezo actuator, and the controller is implemented using FPAAs. As a result, a practical elimination of sensitivity to modeling uncertainty is demonstrated for AM-AFM for similar tracking bandwidth, along with improved imaging performance.

ACKNOWLEDGMENTS

This work was supported by NSF Grant No. CMMI 14-63239.

¹Contact-G. Budget Sensors.

²See <http://www.ni.com/datasheet/pdf/en/ds-151> for Ni X series multifunction data acquisition.

³Family overview, Anadigm, 2003.

⁴Field Programmable Analog Array: AN231K04-DVLP3 - AnadigmApex Development Board (Anadigm, Inc., Campbell, CA, USA, 2006).

⁵See <http://www.asylumresearch.com/probe/ac240ts,olympus> for AC240TS, Olympus.

⁶T. Ando, "High-speed atomic force microscopy coming of age," *Nanotechnology* **23**(6), 062001 (2012).

⁷S. Bains, "Analog's answer to FPGA opens field to masses," *EE Times* **1510**, 1 (2008).

⁸M. Baranwal, "Application of field programmable analog arrays (FPAAs) to fast scanning probe microscopy," M.S. thesis, University of Illinois at Urbana-Champaign, 2014.

⁹M. Baranwal, R. S. Gorugantu, and S. M. Salapaka, "Fast and robust control of nanopositioning systems: Performance limits enabled by field programmable analog arrays," *Rev. Sci. Instrum.* **86**(8), 085004 (2015).

¹⁰G. Binnig, C. F. Quate, and C. Gerber, "Atomic force microscope," *Phys. Rev. Lett.* **56**(9), 930 (1986).

¹¹S. Devasia, E. Eleftheriou, and S. O. R. Moheimani, "A survey of control issues in nanopositioning," *IEEE Trans. Control Syst. Technol.* **15**(5), 802–823 (2007).

¹²J. Comstock Doyle, B. A. Francis, and A. Tannenbaum, *Feedback Control Theory - Chapters 11 and 12* (Macmillan Publishing Company, New York, 1992), Vol. 1.

¹³G. E. Dullerud and F. Paganini, *A Course in Robust Control Theory: A Convex Approach* (Springer Science & Business Media, 2013), Vol. 36.

¹⁴A. J. Fleming, S. S. Aphale, and S. O. R. Moheimani, "A new method for robust damping and tracking control of scanning probe microscope positionning stages," *IEEE Trans. Nanotechnol.* **9**(4), 438–448 (2010).

¹⁵A. Gannepalli, A. Sebastian, J. P. Cleveland, and M. V. Salapaka, "Thermal noise response based control of tip-sample separation in afm," in *Proceedings of the 2004 American Control Conference* (IEEE, 2004), Vol. 4, pp. 3122–3127.

¹⁶F. J. Giessibl, "Advances in atomic force microscopy," *Rev. Mod. Phys.* **75**(3), 949 (2003).

¹⁷K. Glover and D. McFarlane, "Robust stabilization of normalized coprime factor plant descriptions with H_∞ -bounded uncertainty," *IEEE Trans. Autom. Control* **34**(8), 821–830 (1989).

¹⁸MATLAB *Users Guide* (The Mathworks, Inc., Natick, MA, 1998), Vol. 5, p. 333.

¹⁹P. Huang and S. B. Andersson, "High speed atomic force microscopy enabled by a sample profile estimator," *Appl. Phys. Lett.* **102**(21), 213118 (2013).

²⁰G. W. Johnson, *LabVIEW Graphical Programming: Practical Applications in Instrumentation and Control*. *Hauptbd* (McGraw-Hill, 1994).

²¹K. S. Karvinen, M. G. Ruppert, K. Mahata, and S. O. R. Moheimani, "Direct tip-sample force estimation for high-speed dynamic mode atomic force microscopy," *IEEE Trans. Nanotechnol.* **13**(6), 1257–1265 (2014).

²²B. J. Kenton and K. K. Leang, "Design and control of a three-axis serial-kinematic high-bandwidth nanopositioner," *IEEE/ASME Trans. Mechatronics* **17**(2), 356–369 (2012).

²³N. Kodera, D. Yamamoto, R. Ishikawa, and T. Ando, "Video imaging of walking myosin V by high-speed atomic force microscopy," *Nature* **468**(7320), 72–76 (2010).

²⁴C. B. Lee and G. Mohan, "New estimation method of sample properties in dynamic AFM," in *Advanced Materials Research* (Trans Tech Publications, 2013), Vol. 684, pp. 377–380.

²⁵C. Lee and S. M. Salapaka, "Fast robust nanopositioning—A linear-matrix-inequalities-based optimal control approach," *IEEE/ASME Trans. Mechatronics* **14**(4), 414–422 (2009).

²⁶C. Lee and S. M. Salapaka, "Robust broadband nanopositioning: Fundamental trade-offs, analysis, and design in a two-degree-of-freedom control framework," *Nanotechnology* **20**(3), 035501 (2009).

²⁷C. Lee and S. M. Salapaka, "Fast imaging with alternative signal for dynamic atomic force microscopy," *Appl. Phys. Lett.* **97**(13), 133101 (2010).

²⁸L. Ljung, "System identification: Theory for the user," in *PTR Prentice Hall Information and System Sciences Series* (Prentice Hall, New Jersey, 1987), p. 198.

²⁹Y. Luo and S. B. Andersson, "A fast image reconstruction algorithm for compressed sensing-based atomic force microscopy," in *2015 American Control Conference (ACC)* (IEEE, 2015), pp. 3503–3508.

³⁰D. McFarlane and K. Glover, "A loop-shaping design procedure using h synthesis," *IEEE Trans. Autom. Control* **37**(6), 759–769 (1992).

³¹S. O. R. Moheimani, "Invited review article: Accurate and fast nanopositioning with piezoelectric tube scanners: Emerging trends and future challenges," *Rev. Sci. Instrum.* **79**(7), 071101 (2008).

³²M. Napoli, B. Bamieh, and M. Dahleh, "Optimal control of arrays of microcantilevers," *J. Dyn. Syst., Meas., Control* **121**(4), 686–690 (1999).

³³See <http://www.innovative-dsp.com/products.php?product=p25m> for P25M Innovative Integration.

³⁴B. Rogers, L. Manning, T. Sulcik, and J. D. Adams, "Improving tapping mode atomic force microscopy with piezoelectric cantilevers," *Ultramicroscopy* **100**(3), 267–276 (2004).

³⁵D. Rugar and P. Hansma, "Atomic force microscopy," *Phys. Today* **43**(10), 23–30 (1990).

³⁶D. R. Sahoo, T. De Murti, and M. V. Salapaka, "Observer based imaging methods for atomic force microscopy," in *44th IEEE Conference on Decision and Control, 2005 and 2005 European Control Conference. CDC-ECC'05* (IEEE, 2005), pp. 1185–1190.

³⁷S. Salapaka, A. Sebastian, J. P. Cleveland, and M. V. Salapaka, "High bandwidth nano-positioner: A robust control approach," *Rev. Sci. Instrum.* **73**(9), 3232–3241 (2002).

³⁸S. Salapaka, B. Johnson, B. Lundstrom, S. Kim, S. Collyer, and M. Salapaka, "Viability and analysis of implementing only voltage-power droop for parallel inverter systems," in *2014 IEEE 53rd Annual Conference on Decision and Control (CDC)* (IEEE, 2014), pp. 3246–3251.

³⁹S. M. Salapaka, T. De, and A. Sebastian, "New approaches for sample-profile estimation for fast atomic force microscopy," in *ASME 2005 International Mechanical Engineering Congress and Exposition* (American Society of Mechanical Engineers, 2005), pp. 1317–1326.

⁴⁰S. M. Salapaka and M. V. Salapaka, "Scanning probe microscopy," *IEEE Control Syst.* **28**(2), 65–83 (2008).

⁴¹A. Sarwar, P. G. Voulgaris, and S. M. Salapaka, "On the control design and robustness analysis for high-density microcantilever arrays," *J. Vib. Control* **17**, 1195 (2010).

⁴²G. Schitter, R. W. Stark, and A. Stemmer, "Fast contact-mode atomic force microscopy on biological specimen by model-based control," *Ultramicroscopy* **100**(3), 253–257 (2004).

⁴³A. Sebastian and S. Salapaka, "H loop shaping design for nanopositioning," in *American Control Conference, 2003. Proceedings of the 2003* (IEEE, 2003), Vol. 5, pp. 3708–3713.

⁴⁴A. Sebastian and S. M. Salapaka, "Design methodologies for robust nano-positioning," *IEEE Trans. Control Syst. Technol.* **13**(6), 868–876 (2005).

⁴⁵A. C. Shegaonkar and S. M. Salapaka, "Feedback based simultaneous correction of imaging artifacts due to geometrical and mechanical cross-talk

- and tip-sample stick in atomic force microscopy," *Rev. Sci. Instrum.* **78**(10), 103706 (2007).
- ⁴⁶S. Skogestad and I. Postlethwaite, *Multivariable Feedback Control: Analysis and Design - Chapters 2, 5, 8, and 9* (Wiley, New York, 2007), Vol. 2.
- ⁴⁷T. Tuma, W. Haeberle, H. Rothuizen, J. Lygeros, A. Pantazi, and A. Sebastian, "Dual-stage nanopositioning for high-speed scanning probe microscopy," *IEEE/ASME Trans. Mechatronics* **19**(3), 1035–1045 (2014).
- ⁴⁸P. Vettiger, M. Despont, U. Drechsler, U. Dürig, W. Häberle, M. I. Lutwyche, H. E. Rothuizen, R. Stutz, R. Widmer, and G. K. Binnig, "The millipede more than thousand tips for future AFM storage," *IBM J. Res. Dev.* **44**(3), 323–340 (2000).
- ⁴⁹M. Vidyasagar, *Control System Synthesis: A Factorization Approach - Chapter 4* (Morgan & Claypool Publishers, 2011).
- ⁵⁰S. P. Wadikhaye, Y. K. Yong, and S. O. R. Moheimani, "Design and characterisation of a serial-kinematic nanopositioner for high-speed AFM," in *Advanced Intelligent Mechatronics (AIM), 2014 IEEE/ASME International Conference on* (IEEE, 2014), pp. 210–215.
- ⁵¹D. A. Walters, J. P. Cleveland, N. H. Thomson, P. K. Hansma, M. A. Wendman, G. Gurley, and V. Elings, "Short cantilevers for atomic force microscopy," *Rev. Sci. Instrum.* **67**(10), 3583–3590 (1996).
- ⁵²Y. K. Yong and S. O. Moheimani, "Collocated z-axis control of a high-speed nanopositioner for video-rate atomic force microscopy," *IEEE Trans. Nanotechnol.* **14**(2), 338–345 (2015).